

Metal clusters in metal/C₆₀ thin film nanosystems

R. Popescu¹, D. Macovei¹, A. Devenyi¹, R. Manaila^{1,a}, P.B. Barna², A. Kovacs², and J.L. Lábár²

¹ National Institute of Materials Physics, POB MG7, 76900 Bucharest, Romania

² Research Institute for Technical Physics and Materials Science, Budapest, Hungary

Received 5 February 1999 and Received in final form 7 July 1999

Abstract. Structure of metal clusters and of the C₆₀ matrix in Au/C₆₀ and Cu/C₆₀ nanosystems was investigated by X-ray diffraction. Results support a charge-transfer-type interaction at the metal-C₆₀ interface, which affects the size distribution of metal clusters, favouring interstitial location of metal ions in the fullerite lattice.

PACS. 61.48.+c Fullerenes and fullerene-related materials – 61.46.+w Clusters, nanoparticles and nanocrystalline materials – 61.10.-i X-ray diffraction and scattering

1 Introduction

Interaction at the interface between a metal (M) and fullerene C₆₀ is presently the object of many experimental and theoretical investigations [1]. It includes two aspects:

- 1) charge transfer (generally from the metal towards C₆₀, as required by the energy difference between the Fermi level of the metal and the LUMO orbitals of C₆₀) [2–8];
- 2) formation of hybrid metallic orbitals [9–12].

The evidence for charge transfer mainly comes from the shift of Raman frequencies which allows, with due calibration, an estimation of the average charge transferred to a C₆₀ molecule [2,3]. Also, the decrease in intensity of the X-ray absorption (XAS) transition to the LUMO band [5,7] supports the negative charging of C₆₀, as does the apparition of LUMO-derived occupied states in UV photoemission spectra [4]. On the other hand, alteration of density of states (DOS) distribution in M/C₆₀ systems, as compared with pure C₆₀ samples [1] suggests formation of metallic hybrid orbitals, of both bonding and anti-bonding character.

M/C₆₀ interface interaction was usually studied in planar systems (bi-and multilayers). On the other hand, a nano-dispersion of the metal in the fullerite C₆₀ matrix looks more promising for studying the interface interaction, due to the much higher specific interface. Such nano-dispersions can be obtained as co-evaporated thin films. Their properties (electrical transport, optical) are expected to depend on the dispersion degree of the metal clusters, but also on their structure and on that of the C₆₀ matrix. The effects of interface interaction must show up in all of these properties and M/C₆₀ nanosystems look most appropriate for investigating them.

Recent calculations performed in a rigid-band model [13,14] showed that charge transfer determines, *via* the cohesive, surface and Coulomb energies, the range of cluster sizes which are energetically stable. The present work intends to investigate the structure of both metallic clusters and C₆₀ matrix in Au/C₆₀ and Cu/C₆₀ thin-film nanosystems, looking for effects of the interface interaction. As widely accepted in literature, charge transfer is higher in the Cu/C₆₀ system (1.5–2.0 e⁻/C₆₀ [7]) than in the Au/C₆₀ one (1 ± 1e⁻/C₆₀) [2].

2 Experimental

M/C₆₀ films (0.3–3 μm thick) were prepared by co-depositing metal (99.5% purity) and C₆₀ (99.99% purity) from two independently-controlled sources, after proper calibration of the evaporation rates. The temperature of the C₆₀ source was between 450–550 °C. Substrates included Si (111) and Si (100) wafers (for XRD and EDS) and KBr (for TEM and ED) in the case of Au/C₆₀ films. For Cu/C₆₀ samples fused silica substrates were used, in order to avoid the high-energy harmonics diffracted on the (111) Si planes, which lie close to the Au (200) and Cu (200) lines. Cu/C₆₀ films were prepared in two runs (Tab. 1). Samples B were obtained with a better control over the deposition rates for both C₆₀ and metal and in a vacuum better than 2 × 10⁻⁶ torr, allowing a lower growth rate (10 nm/min instead of 10² nm/min in series A).

The average composition of the Cu/C₆₀ films was determined by Elastic Recoil Detection Analysis (ERDA) or Energy Dispersive X-ray Spectrometry (EDS) (Tab. 1). For the Au/C₆₀ nanosystems, EDS was performed in transmission mode of electron microscopy (TEM) yielding the local metal content, which was averaged over at least two spots. Average compositions M_xC_{100-x} are shown

^a e-mail: manaila@alpha1.infim.ro

Table 1. Thickness and average metal (M) content x in M_xC_{100-x} M/C₆₀ films (M = Au, Cu). Local concentrations from EDS data are somewhat depth-dependent and differ by at most ± 0.5 at.% from the given average values.

System	Sample	Thickness (μm)	Metal x (at.%)	Method
Au/C ₆₀	A1	3	1.7	EDS
	A2	1.3	4.5	EDS
	A3	0.3	2.4	EDS
Cu/C ₆₀	Series CA1	1.1	0.6	EDS
	A	1.3	1.5	EDS
	CB1	1.5	13.3	ERDA
	Series CB2	0.7	13.0	ERDA
	B	2.3	35.7	ERDA

in Table 1. For the Au/C₆₀ films, cross-sectional TEM (XTEM) allowed to estimate the depth homogeneity of metal concentration, as well as the size distribution of metal clusters [15].

The diffraction patterns of the M/C₆₀ films were taken using both sealed-tube X-ray radiation ($\text{CuK}\alpha$) and synchrotron radiation source ($\lambda = 1.0395 \text{ \AA}$ and 1.0421 \AA). The synchrotron data were taken at the Daresbury Synchrotron Radiation Laboratory (UK). Line profile analysis was performed with dedicated programs, using Voigt profiles. As prescribed by single-line profile analysis [16], the Lorentz component of the broadening was ascribed to the limited coherence length D_{eff} , while the Gaussian component was used to estimate average lattice distortions $\langle \varepsilon \rangle^{1/2}$. Separation of Lorentz and Gauss broadening components depends upon the Voigt parameter φ (ratio between FWHM and integral width β). This descriptor of the Voigt profile is influenced by the shape of line tails. These zones are difficult to measure precisely for faint and broad lines, when background details become relatively important. Therefore, for weak lines the uncertainty in D_{eff} and $\langle \varepsilon^2 \rangle$ is expected to increase. Raw linewidths were applied a Rachinger correction (whenever $\text{CuK}\alpha$ radiation was used). Also, correction for instrumental width was performed, using the lines of the Si single-crystal substrate or of an α -quartz external standard. This correction amounted to at most 10% of the raw linewidth. Whenever single-line analysis was used, instrumental correction was separately applied to the two linewidth components. The background was approximated by polynomials up to the second degree.

3 Results

3.1 Microstructure

XTEM data were collected with a Philips microscope on ion-thinned samples. In Au/C₆₀ films, Au nanoclusters were noticed with average size between 1.5 and 7 nm, for $\text{Au}_x\text{C}_{100-x}$ compositions with $x > 0.4$ [15]. Metal clusters were also noticed in Cu/C₆₀ films, with average sizes of 2–13 nm. HREM images of the sample with $x = 0.6$ (Fig. 1) revealed crystalline Cu clusters, where the (111) planes are clearly visualized. Details about the microstructure of Cu/C₆₀ films will be given elsewhere.

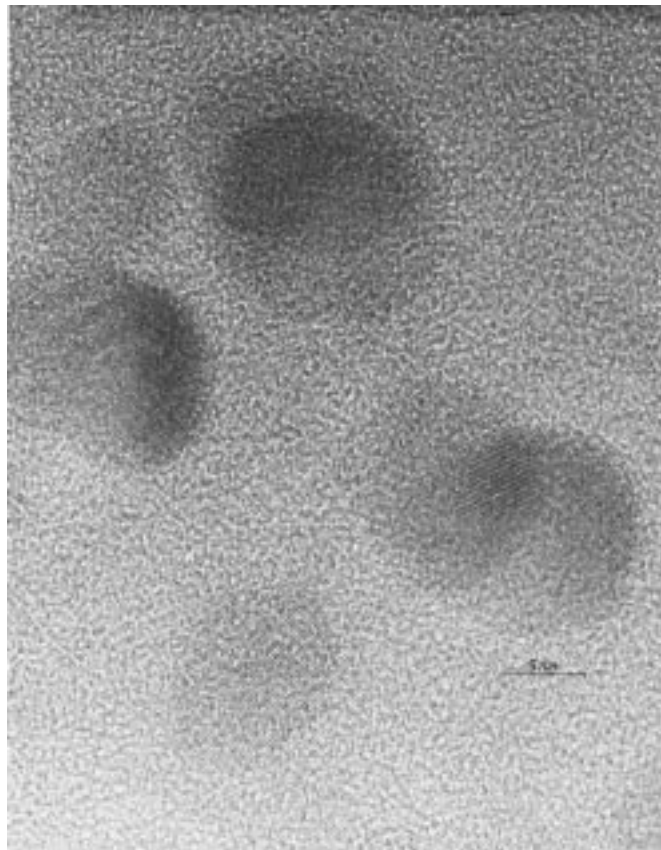


Fig. 1. HREM micrograph of a $\text{Cu}_x\text{C}_{100-x}$ film ($x = 0.6$), showing crystalline Cu clusters.

3.2 Size and distortion state of metal clusters

Diffraction lines of the fcc metals Au and Cu were only discernible above a critical metal content. Metal line (111) was measurable on all of the samples in Table 1. However, the (200) line was accessible only in some samples, while in Au/C₆₀ films on Si (111) substrates it was often superposed with spurious harmonic contributions (see Sect. 2). Further diffraction details of Cu and Au could not be recorded, due to the limited film thickness. Figure 2 shows typical diffraction patterns contributed by metal clusters in both systems. Single-line profile analysis applied to both (111) and (200) lines resulted in D_{eff} and

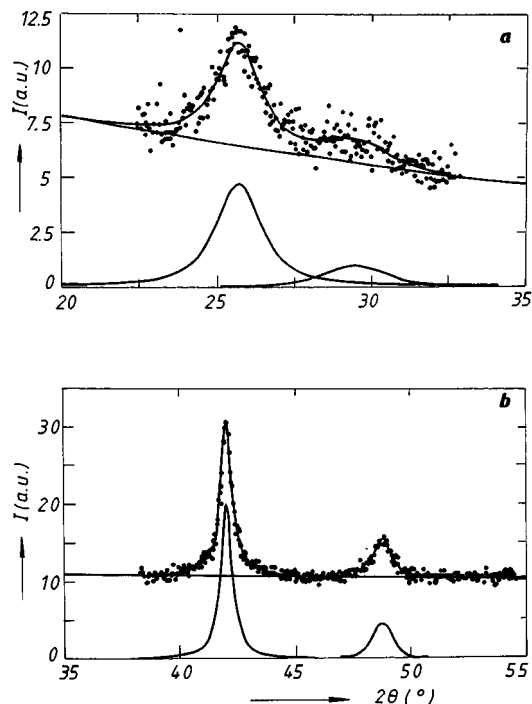


Fig. 2. Fragments of diffraction patterns with details from Au (a) and Cu (b) clusters. (a) $\lambda = 1.0421$ Å; (b) $\lambda = 1.54178$ Å. Lines (111) and (200) of the metal are shown.

$\langle \varepsilon^2 \rangle$ values. Separate analysis of the two lines was considered advisable in our case because comparison of the results can decide on the polycrystalline or quasi-amorphous structure of metal clusters.

Figure 3 shows $1/D_{\text{eff}}$ for the metal clusters in Au/C₆₀ and Cu/C₆₀ nanosystems, as derived from the most intense (111) line. The values measured with conventional source and synchrotron radiation generally differ little (except sample A1) (Fig. 3a). Taking into account the uniform algorithm of data reduction, these differences are believed to originate in sample inhomogeneity, as different parts of the film surface were irradiated at the two radiation sources. Also, for weak lines the determination of D_{eff} and $\langle \varepsilon^2 \rangle$ is subject to increased uncertainty (see Sect. 2). The $1/D_{\text{eff}}$ values in Cu/C₆₀ films are definitely higher (smaller crystallite size) than in a reference Cu film (Fig. 3b). The difference between the Cu film and sample CB3 (with the highest Cu content, see Tab. 1 and Fig. 3b) marks the experimental error.

The $1/D_{\text{eff}}$ values, which measure the dispersion state of metal clusters, do not show a coherent dependence on metal content, if the above-mentioned differences between data are taken into account. Therefore, we feel entitled to compare the average $1/D_{\text{eff}}$ values for Cu/C₆₀ and Au/C₆₀ films for metal concentrations in the range 0.6-13 at.%. The average values are $13.1 \times 10^{-3} \text{ \AA}^{-1}$ and $20.4 \times 10^{-3} \text{ \AA}^{-1}$ for Cu and Au clusters, respectively, suggesting a somewhat smaller coherence length of Au clusters in comparison with the Cu ones.

The D_{eff} values (synchrotron data) for Au/C₆₀ films A1 and A2 are 32 and 40 Å respectively, as derived from

the (111) line width. They are slightly lower than the average TEM diameter of 56 Å (film A1) and 68 Å (film A2) [15] (Fig. 3a).

Lattice distortions in metal clusters (Fig. 4) show differences between Cu- and Au-containing samples. Cu clusters in samples B appear more disordered than in the other (A) deposition batch. However, Cu clusters are on the average much less distorted than Au ones (average distortion $\langle \varepsilon^2 \rangle^{1/2}$ over all samples is 2.5×10^{-3} for Cu *vs.* 5.4×10^{-3} for Au, as derived from the (111) line widths). The high crystallinity of Cu clusters is also confirmed by the HREM images (Fig. 1).

The $1/D_{\text{eff}}$ and $\langle \varepsilon^2 \rangle$ values derived from both (111) and (200) metal lines are expected to be similar for polycrystals with quasi-spherical crystallite morphology. For highly distorted crystallites, a slight increase of $\langle \varepsilon^2 \rangle$ is expected for (200) over that of the (111) line, on account of static phonon disorder. This is indeed the case for the Cu clusters (Fig. 4b). On the other hand, (200) lines in Au clusters yield $\langle \varepsilon^2 \rangle^{1/2}$ values which are consistently higher than those resulting from the (111) lines (Fig. 4a). This behaviour speaks for a quasi-amorphous character of Au clusters in Au/C₆₀ films, as we already reported in [15] and is visible on Figure 2a. This assertion is supported by the different values of Au lattice parameter derived from the two diffraction lines (see Sect. 3.3).

3.3 Lattice parameter of metal clusters

Metal nanostructures were often reported to have altered lattice parameters, as required by the modified equilibrium at interfaces with the matrix. In Au/C₆₀ films, the Au clusters systematically showed a decreased lattice parameter, as referred to the bulk value. Variations $\Delta a = -(0.2 - 0.8)\%$ were derived for different samples, on the basis of (111) corrected positions. Internal (Si substrates) or external (α -quartz single crystal) standards were used to correct for systematical errors in line peak position. However, line (200) consistently yielded positive values for Δa , being located at too small angles. The variation of the lattice parameter, as derived from (111) and (200) lines differed by 0.6-0.7%, beyond the experimental uncertainty. This observation supports the quasi-amorphous character of Au clusters.

On the contrary, Cu clusters in Cu/C₆₀ films display a lattice parameter a_{Cu} increase of 0.2-0.6% for different samples (average results from (111) and (200) lines, both differing by at most 0.2% and having the same sign). Sample CB3, with the highest Cu content and very large metal particles (Figs. 1 and 3b), was excluded from the average over the a_{Cu} values. The agreement between lattice parameter and $\langle \varepsilon^2 \rangle^{1/2}$ values yielded by both diffraction lines supports a true polycrystalline nature of the Cu clusters.

3.4 Structure of the fullerite C₆₀ matrix

The disorder state of the C₆₀ fcc matrix was found to be different in Au/C₆₀ and Cu/C₆₀ film nanosystems.

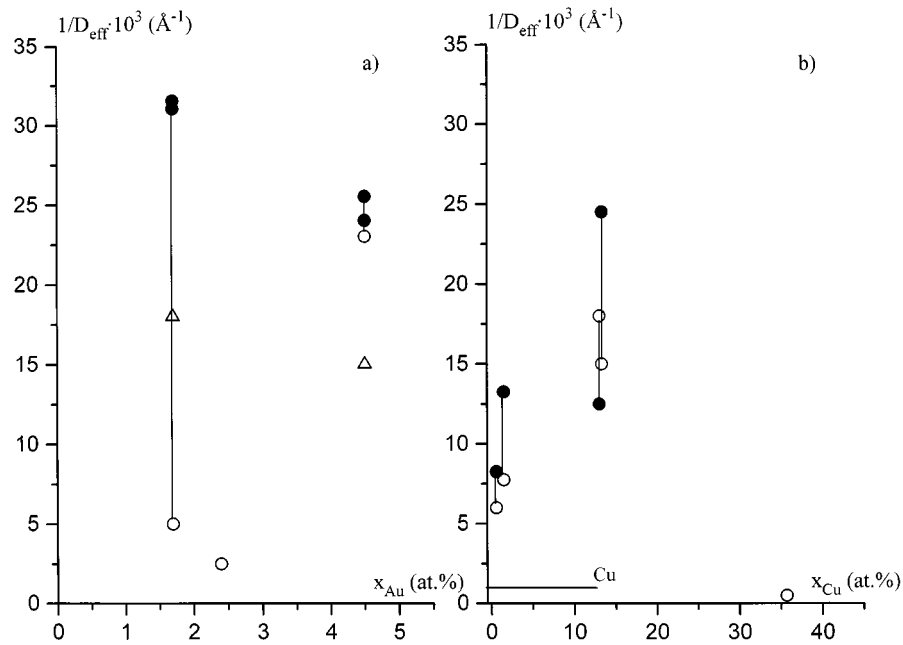


Fig. 3. Inverse coherence length $\frac{1}{D_{\text{eff}}}$ for Au (a) and Cu (b) clusters in metal/ C_{60} films. Integral (111) linewidths were used. (●) synchrotron radiation data. (○) sealed-source data ($\text{CuK}\alpha$). (Δ) average TEM size [15]. Synchrotron data are occasionally given for two wavelengths (two symbols). Cu: reference Cu film. Data belonging to the same sample are connected by vertical bars.

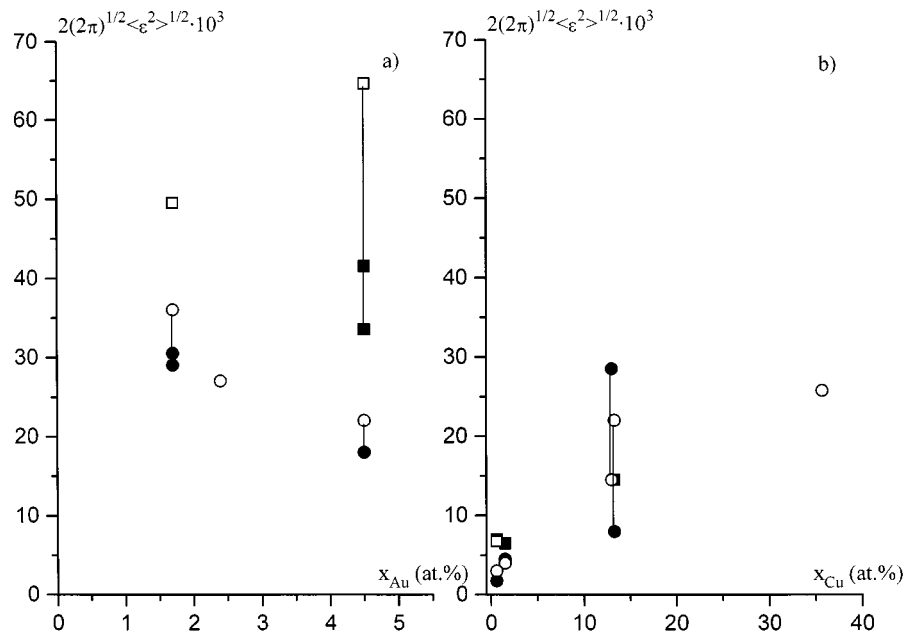


Fig. 4. Lattice distortions $2(2\pi)^{1/2}\langle\varepsilon^2\rangle^{1/2}$ for Au (a) and Cu (b) clusters. (●, ○) (111) line, synchrotron and sealed-source data, respectively. (■, □) (200) line, synchrotron and sealed-source. Data belonging to the same sample are connected by vertical bars.

Although deposition conditions were kept as similar as possible in Au/C₆₀ and Cu/C₆₀ film preparation, slight differences in the evaporation rate of C₆₀ cannot be excluded. However, in our opinion, the differences between the fullerite state in the two systems are too large to be accounted for by preparative details and have to be related to the nature of the metal, *i.e.* to the metal-C₆₀ interface interaction.

Diffraction lines of fcc C₆₀ could be noticed, on better-structured samples, up to (511) ($k \cong 0.37 \text{ \AA}^{-1}$, $k = 2 \frac{\sin \theta}{\lambda}$). However, due to the attenuation factor related to film thickness, our conclusions will be mainly based on the relatively intense (220) and (311) peaks. The (111) C₆₀ reflection showed in most films the low-angle satellite, indicative of stacking faults [17].

Figures 5a and 5b show the corrected FWHM linewidths for C₆₀ (220) and (311) lines in Au/C₆₀ and Cu/C₆₀ films, respectively. No attempt was made to separate linewidth in Lorentz and Gauss components, for reasons which will be given below. Linewidths of C₆₀ in Au/C₆₀ (Fig. 5a) are in the range of values found for pure C₆₀ films, prepared in the same conditions and show no coherent variation with metal content. The (220) and (311) lines are relatively strong, which allows a reliable determination of the profile shape (Voigt factor φ). The measured Voigt factor is remarkably constant at 0.67-0.70 in all the four Au/C₆₀ samples, for both (220) and (311) lines. This constancy speaks for a polycrystal nature of C₆₀. Also, the relatively low φ value (close to the ideal Lorentz 0.6366) shows that line broadening is almost exclusively due to limited coherence length D_{eff} . Application of a simple Scherrer formula $D_{\text{eff}} = 1/\Delta k$ to the (220) and (311) C₆₀ linewidths in Au/C₆₀ films results in an average D_{eff} of 3.8 ± 0.7 nm.

In Cu/C₆₀ films, C₆₀ linewidths are significantly higher than in Au/C₆₀ and in pure C₆₀ (Fig. 5b) which, in some cases, causes the lines to be merged in the background. Also, line areas are lower, inducing an increased uncertainty in the shape factor φ . Anyway, the range of φ values is 0.67-0.94 for both (220) and (311) lines in Cu/C₆₀, as compared with 0.67-0.70 for the fullerite in Au/C₆₀ films. The increase of the shape factor towards the 0.9394 value, typical for Gauss profiles, suggests that significant distortions occur in the fullerite matrix, in presence of Cu clusters. Again, no clear correlation can be established between linewidths and metal concentration in the prepared range (Fig. 5b), if differences between sealed-source and synchrotron data are taken into account. This is valid for fullerite in Cu/C₆₀ films of both series (Tab. 1).

The ratio of (220) to (311) C₆₀ line areas (A) deserves a special comment. In six pure C₆₀ films, this ratio covers the range 0.6-1.6. The rather divergent values can be explained by the weak signal due to the small film thickness. Also, uncertainty in the decomposition of the (311) + (222) partially superposed profiles contributes to this variation. A similar range of A(220)/A(311) ratios was found in Au/C₆₀ films (0.7-1.0). On the other hand, significantly lower values were occasionally measured for the fullerite in Cu/C₆₀ films, where the range of values for

this ratio is 0.2-1.1, with five out of eight samples falling below 0.7. The reduced relative areas of the (220) line in some samples does not correlate with particularly large C₆₀ linewidths.

This reduction of A(220) was accounted for in our calculations of C₆₀ line intensities, with partial occupation of tetrahedral and/or octahedral interstices by Cu atoms (especially for interstices of the former type, also twice as numerous as the octahedral ones). Ratios in the observed range could be obtained in this way [18]. However, these interstitials also would give rise to non-zero (200) and (400) lines which, in a perfect and pure C₆₀ fcc lattice are cancelled by the minima of the cage form factor. The (200) line should reach 63% (13%) of the (311) one for complete occupation of tetrahedral (octahedral) interstices (actual ratios should be even higher if corrections for film thickness were considered). Uncertainties in area measurement, caused by the weak and broad diffraction details, prevent such observations.

We might ask if the lattice parameter of fullerite is also affected by the presence of the metal (or by the induced distortions). A pure C₆₀ film showed a lattice dilation of 0.2%, which can be easily accounted for by defects and/or elastic stresses. On the other hand, in Cu/C₆₀ films the fullerite lattice displays a much higher dilation (0.9-1.6%, sample CB3 being again excluded). For the non-distorted fullerite in Au/C₆₀ films, this dilation ranges from 0.4 to 0.7% only, notwithstanding the Au⁺ radius being larger than that of Cu⁺ (see Sect. 4). We can conclude to the fact that dilation of the C₆₀ lattice is related to its degree of distortion.

4 Discussion and conclusions

The Au/C₆₀ and Cu/C₆₀ film nanosystems differ, from a structural point of view, in two main points:

- Au nanoclusters are smaller than Cu ones (also more disordered, qualifying for a quasi-amorphous description);
- fullerite in Au/C₆₀ films is unaffected by the presence of the metal, being similar to the pure C₆₀ films as concerns linewidths and profile shapes. By contrast, fullerite in Cu/C₆₀ films shows broader diffraction lines, the extra broadening being mainly caused by lattice distortions.

The apparent relation between nature of the metal and C₆₀ matrix structure is offered an explanation based on the stability of metal clusters in the presence of interface interaction. Calculations of the total cluster energy E_a [13,14,18], taking into account different volume and surface terms showed (Fig. 6) that metal clusters display a critical radius R_C . Clusters above this size tend to grow, reducing E_a , till it becomes negative. Clusters below R_C are unstable with respect to the growth process and tend to decompose. This rigid-band model, mainly based on charge transfer (which lowers the surface energy), is justified by the Au/C₆₀ and Cu/C₆₀ interface interaction being predominantly ionic [1]. The decomposition process

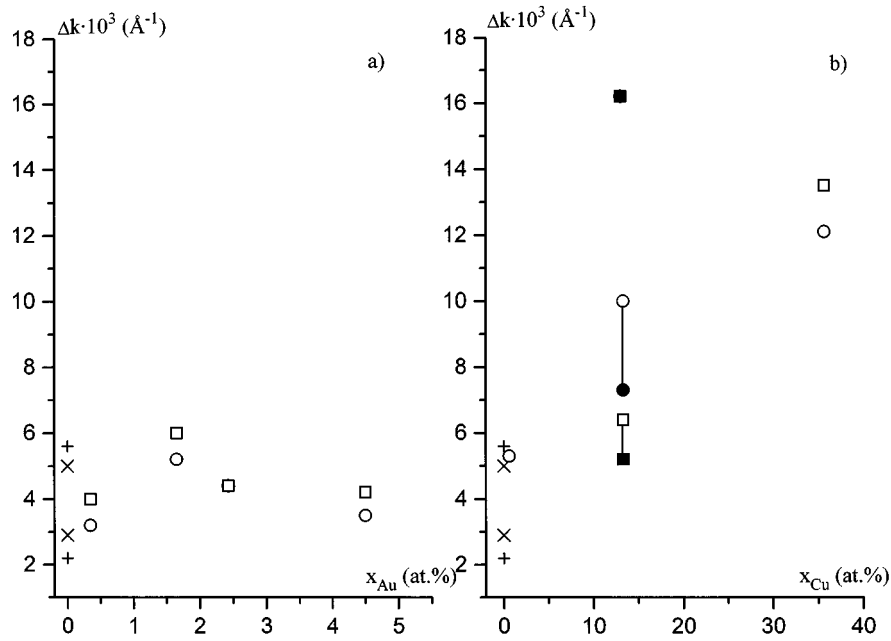


Fig. 5. FWHM data Δk for (220) (●, ○) and (311) (■, □) fullerite lines in Au/C_{60} (a) and Cu/C_{60} (b) films. Empty symbols: sealed-source. Full symbols: synchrotron source data. (×, +) (220) and (311) lines in two pure C_{60} films. Data belonging to the same sample are connected by vertical bars. $k = 2(\sin \theta)/\lambda$.

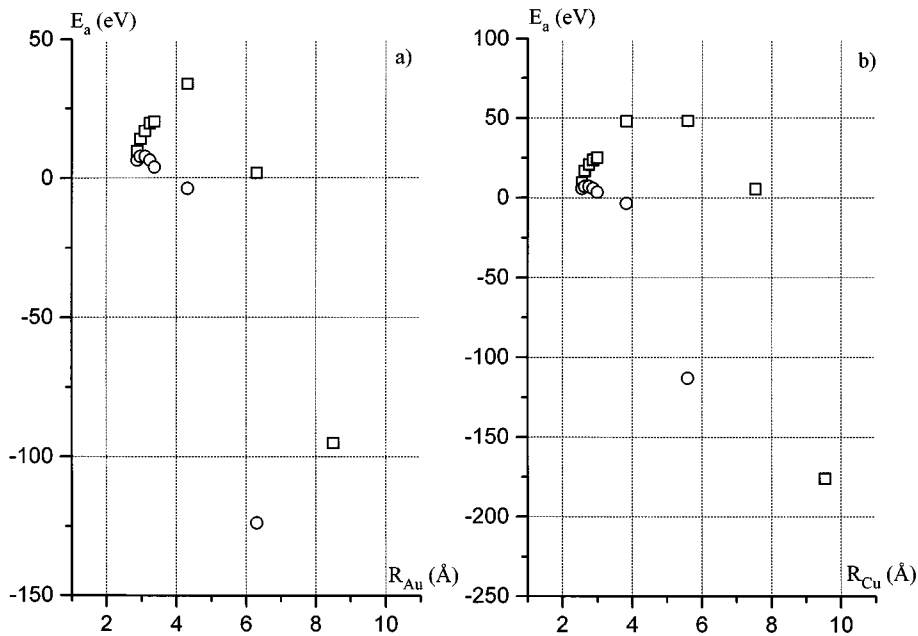


Fig. 6. Total energy of the metal clusters E_a vs. radius R of the clusters for Au (a) and Cu (b). (○) without interface charge transfer; (□) with interface charge transfer.

can go far, up to having metal ions (or very small ionic aggregates) located on interstitial sites of the C_{60} lattice. The radii of these interstices are 1.12 Å (tetrahedral) and 2.06 Å (octahedral), allowing insertion of small ionized atoms ($R_{\text{Au}^+} = 1.37 \text{ \AA}$, $R_{\text{Cu}^+} = 0.96 \text{ \AA}$).

The critical size R_C depends on the charge transfer Q_f at the metal/ C_{60} interface (Fig. 6), increasing at higher Q_f [13, 14, 18]. The reason for this dependence is the highly

positive Coulomb energy, dominant at small cluster size. Theoretical evaluations [18] yielded $2R_C$ values of 0.8 nm and 1.0 nm for Au and Cu, respectively.

In Au/C_{60} nanosystems, with lower charge transfer, a range of cluster values was found by TEM [15], with average size D of 1.5 to 7 nm, increasing with increasing metal content. These D values can be considered as averages over cluster sizes in the “stable” $R > R_C$ range. On the other

hand the small, unstable Au clusters with $R < R_C$ seem to exert no structural influence on the fullerite matrix. The C₆₀ lattice appears unaffected by the Au clusters, which cause little lattice strain (the observed strain $\langle \varepsilon^2 \rangle$ is comparable to that induced by stacking faults and impurities in pure C₆₀ films).

However, in the Cu/C₆₀ system the charge transfer is higher and R_C slightly increases [13,14,18]. Higher minimal D values of Cu clusters are expected and indeed observed (2-3 nm from TEM micrographs of samples CA1 and CA2 [19]). The concentration of unstable nuclei should now be higher than in case of Au. They apparently decompose into (Cu⁺)_{*n*} ion aggregates (or ions), which penetrate on the interstices of the C₆₀ lattice, causing strong distortions. Recently, evidence for interstitial location of Cu and Au ions was found from EXAFS experiments [20], particularly strong in the case of Cu/C₆₀ nanosystems.

Also Raman spectroscopy revealed evidence for negative charging of the C₆₀ matrix. The intramolecular Ag(2) mode at 1470 cm⁻¹ showed [3], for sample CB3 with the highest Cu content, a satellite at ~ 1448 cm⁻¹. The magnitude of the negative frequency shift suggests it originates in zones with approximate composition Cu₃C₆₀, where octahedral and tetrahedral fullerite interstices would be completely occupied by ionized Cu.

The smaller size of the Cu⁺ ion, as compared with the Au⁺ one (see above) can also favour interstice occupancy by the former.

Another fact supporting interstitial location of Cu⁺ ions is the dilation of fullerite lattice in Cu/C₆₀ films being higher than in Au/C₆₀ samples (see Sect. 3.4.).

We can conclude that dilation and distortion of the C₆₀ lattice are both caused by a fraction of interstitial metal ions, especially in Cu/C₆₀ nanosystems.

The quantitative details of our model [13,14,18] sensitively depend on the cohesion energy of the metal and on the transferred charge Q_f . It is also necessary to remind that calculations were performed in a rigid-band scheme, ignoring the possible formation of hybrid metal-C₆₀ orbitals, which would further reduce the surface energy of clusters, favouring metal dispersion.

It is worth mentioning that Al/C₆₀ nanosystems, prepared as co-evaporated thin films with 4.15 at.% Al on NaCl (001) substrates at room temperature [21] showed no evidence of Al particles in high-resolution TEM or ED observations. This suggests a highly dispersed state of Al within the C₆₀ matrix, possibly related to the formation of predominantly covalent bonds with C₆₀, of intermediate strength [1]. Nevertheless, the softening of the Ag(2) Raman mode [21] signals that some charge transfer also occurs, apparently proportional to the specific interface area.

We can conclude to the fact that charge transfer at the metal/C₆₀ interface influences the size of the metal clusters and can favour interstitial location of very small ionized clusters or metal ions. The necessary condition for a high metal dispersion is a charge transfer large enough to counteract the cohesive energy by electrostatic terms.

Application of the same model to virtual K/C₆₀ nanosystems pointed [18] to a high concentration of small, unstable K clusters, explaining the well-known tendency of A_{*x*}C₆₀ (A = alkalis) to form interstitial compounds. Our data suggest that ion location on interstitial C₆₀ sites is also possible for post-transition metals (Au, Cu) and is favoured by interface charge transfer. Also, the ratio between ionic radii and interstice size should be an important factor in this respect.

One of us (A.D.) is highly indebted to the Alexander von Humboldt-Foundation for gracious and continuous financial support.

References

1. A.J. Maxwell, P.A. Brühwiler, D. Arvanitis, *Phys. Rev. B* **57**, 7312 (1998).
2. M.R.C. Hunt, S. Modesti, P. Rudolf, *Phys. Rev. B* **51**, 10039 (1995).
3. R. Manaila, A. Belu-Marian, D. Macovei *et al.*, *J. Raman Spectroscopy* (1999, in press).
4. S.J. Chase, W.S. Bacsá, M.G. Mitch *et al.*, *Phys. Rev. B* **46**, 7873 (1992).
5. E. Rowe, P. Rudolf, L.H. Tjeng *et al.*, *Int. J. Mod. Phys. B* **6**, 3909 (1992).
6. G.K. Wertheim, D.N. Buchanan, *Phys. Rev. B* **50**, 11070 (1994).
7. K.-D. Tsuei, J.-Y. Yuh, C.-T. Tzeng *et al.*, *Phys. Rev. B* **56**, 15412 (1997).
8. G.K. Wertheim, D.N. Buchanan, *Solid State Commun.* **88**, 97 (1993).
9. A.J. Maxwell, P.A. Brühwiler, A. Nilsson *et al.*, *Phys. Rev. B* **49**, 10717 (1994).
10. A.J. Maxwell, P.A. Brühwiler, S. Andersson *et al.*, *Phys. Rev. B* **52**, R5546 (1995).
11. C. Cepek, A. Goldoni, S. Modesti, *Phys. Rev. B* **53**, 7466 (1996).
12. A.F. Hebard, C.B. Eom, Y. Iwasa *et al.*, *Phys. Rev. B* **50**, 17740 (1994).
13. R. Popescu, D. Macovei, A. Devenyi *et al.*, *Full. Sci. Technol.* **7**, 77 (1999).
14. R. Popescu, D. Macovei, A. Devenyi *et al.*, in *Proc. 6th European Conference on Powder Diffraction EPDIC6, Aug. 1998, Budapest, Hungary*, Mater. Sci. Forum **321-324**, 554 (1999).
15. A. Devenyi, R. Manaila, A. Belu-Marian *et al.*, *Thin Solid Films* **335**, 258 (1998).
16. J.J. Langford *et al.*, *Aust. J. Phys.* **41**, 173 (1988).
17. M. Mănciu, R. Manaila, A. Devenyi *et al.*, *Full. Sci. Technol.* **2**, 255 (1994).
18. R. Popescu (unpublished results).
19. P.B. Barna (personal communication).
20. D. Macovei, R. Popescu, R. Manaila, B.R. Orton, in *Daresbury Laboratory, Synchrotron Radiation Dept., Scientific Reports 1996-97*, 1998, p. 368; D. Macovei, R. Manaila, D. Fratiloiu *et al.*, in *Daresbury Laboratory, Synchrotron Radiation Dept., Scientific Reports 1997-98* (to be published).
21. J.G. Hou, Y. Li, Y. Wang *et al.*, *Phys. Stat. Sol. A* **163**, 403 (1997).